THE EFFECT OF WELD LINE ORIENTATION AND MECHANICAL INTEGRITY OF FRICTION-STIR WELDED TAILORED BLANKS MADE FROM PRIMARY AND RECYCLED AA6082 EXTRUSIONS

Yugesh Raajha MS, Geir RINGEN, Øystein GRONG, Torgeir WELO

Norwegian University of Science and Technology – Department of Mechanical and Industrial Engineering, 7491, Trondheim, Norway, yugesh.raajha@ntnu.no

https://doi.org/10.37904/metal.2025.5091

Abstract

Recycled aluminum in tailor-welded blanks (TWBs) offers sustainable solutions for automotive applications. However, variations in impurity levels, depending on the source of the scrap, negatively impact weldability with conventional fusion-based welding methods, limiting its usage compared to primary aluminum. This study aims to investigate how differences in microstructural and mechanical anisotropy between primary and recycled 6082-T6 aluminum alloys affect the mechanical integrity of TWBs joined through friction stir welding (FSW). The alloys differ in chemical composition, particularly with the recycled variant showing elevated levels of iron (Fe), copper (Cu), and zinc (Zn), which can significantly influence weldability, microstructure, and mechanical performance. Both alloys were welded together at a rotational speed of 1000 rpm and a welding speed of 60 mm/min, with weld line orientations of 0°, 45°, and 90° relative to the extrusion direction. Before welding, tensile tests were conducted to evaluate the strain characteristics in different directions, determining the alloys' mechanical anisotropy. Results show clear differences in the mechanical anisotropy between primary and recycled aluminum, primarily due to the variation in the distribution and density of intermetallic phases across the thickness. The stir zone (SZ) exhibited a reduced yield strength of 195 MPa, which resulted in an increased fracture strain of 29%. This is attributed to the dissolution of strengthening precipitates and the homogeneous distribution of intermetallic particles within the matrix. The recrystallized grains within the SZ were equiaxed and significantly finer than the base metals (BMs), with an average grain size of approximately 7 ± 3 μm compared to 20 ± 5 μm in the BMs. The hardness in the SZ was found to be significantly lower than in the BMs, with maximum hardness values ranging between 70 – 90 HV for all three orientations. However, the transverse tensile properties were largely unaffected by the weld line orientation, resulting in consistently lower strength and ductility values compared to those of the BMs.

Keywords: Friction stir welding, anisotropy, recycled aluminum, dynamic recrystallization

1. INTRODUCTION

Friction Stir Welding (FSW) has gained significant attention due to its ability to weld a variety of aluminum alloys by reducing gas porosity, element segregations, residual stresses, and distortion common in traditional fusion welding techniques [1, 2]. It differs from other welding processes in that it involves joining metals in the solid state condition through severe plastic deformation at high strain rates in front of the rotating tool. Unlike conventional welding, heat generation and transport in FSW are assisted by this plastic flow, resulting in dynamic recrystallization (DRX) behavior within the stir zone (SZ) [3-5]. Because of these unique features, FSW of recycled aluminum is attractive due to its high oxide and impurity tolerance, made possible by a process temperature that is sufficiently low to prevent local melting [6].

FSW of Tailor-welded blanks (TWBs) are widely used in the transportation sector to manufacture lightweight, high-strength, and corrosion-resistant components, enhancing fuel efficiency and reducing emissions [7].

TWBs enable the strategic placement of similar or different materials to optimize strength, weight distribution, and part performance [8]. The differences in mechanical properties of recycled aluminum compared to primary aluminum extrusions can be leveraged by selectively designing the placement of both materials and joining them through FSW. These property differences are largely influenced by variations in chemical composition, particularly higher levels of impurity elements such as Fe, Cu, and Zn, in recycled aluminum, which arise from the heterogeneous nature of scrap sources. Such compositional variations can affect not only mechanical performance but also weldability and microstructural evolution during processing. In a previous study by the authors [9], FSW of primary *vs.* recycled AA6082 was conducted, offering detailed insights into the effect of base metal temper condition on the weldability. Failure occurred in the heat-affected zone (HAZ) region located within primary aluminum, and differences could be found in terms of ductility and strength between the different tempers. A natural follow-up of this work is to examine how the orientation of the weld line relative to the extrusion direction affects the heat flow, residual stress distribution, and subsequent formability. Past studies using other welding methods suggest that this variation plays a key role in determining the mechanical properties, especially in joining dissimilar aluminum alloys [10].

The objective of this work is to bridge the above knowledge gap by systematically investigating the impact of weld line orientation on friction-stir welded tailored blanks made from both primary and recycled AA6082 extrusions. In addition, the study will explore the microstructure evolution and mechanical behavior within the SZ of the welds, examining how variations in orientation affect the overall structural and mechanical integrity of TWBs.

2. EXPERIMENTAL PROCEDURES

2.1 Materials and methods

Primary (GA1) and recycled (GA3) AA6082-T6 extrusions in the form of hollow trapezoidal profiles (7 m long, 83 mm wide, 2.6 mm thick) were used as the base metals (BMs) for the FSW experiments. Their chemical compositions are given in **Table 1**. The details of the extrusion process have already been provided in the previous study [11]. Rectangular strips, approx. 60 mm wide, were cut on one of their faces using water jet cutting. Subsequently, the edges were milled straight to ensure precise weld fit-up. Prior to FSW, the surfaces to be joined were scrubbed mechanically and cleaned with ethanol to remove any surface contaminants.

The welding operation was performed using an HT-JM16 x 8/1 FSW machine, employing a truncated cylindrical H13 tool steel featuring a 2.5 mm long pin and an 11 mm wide shoulder. The sheet preparation and experimental setup are shown in **Figure 1(a)** & **1(b)**, respectively. The welding was done in displacement control mode, using a rotational speed of 1000 rpm, a welding speed of 60 mm/min, and a tool tilt angle of 2.5°. These process parameters were optimized after a series of iterative trials and used in the subsequent fabrication of the TWBs. The same welding parameters were employed for all three weld line orientations. In the first TWB, the extrusion direction (ED) of the base metals is parallel to the weld line, referred to as WL || ED; i.e., the orientation angle between the weld line and extrusion direction is 0°. Successively, TWBs with the ED perpendicular to the weld line (referred to as WL ⊥ ED) and with ED oriented 45° with respect to the weld line, referred to as WL / ED, were fabricated.

Table 1 Chemical composition of the primary and recycled AA6082-T6 extrusions used in the FSW trials (wt%)

AA6082 - T6	Si	Fe	Cu	Mn	Mg	Zn	Ti	Al
Primary (GA1)	0.9	0.22	0.02	0.55	0.65	0.02	0.01	Balance
Recycled (GA3)	0.9	0.32	0.1	0.55	0.65	0.2	0.01	Balance

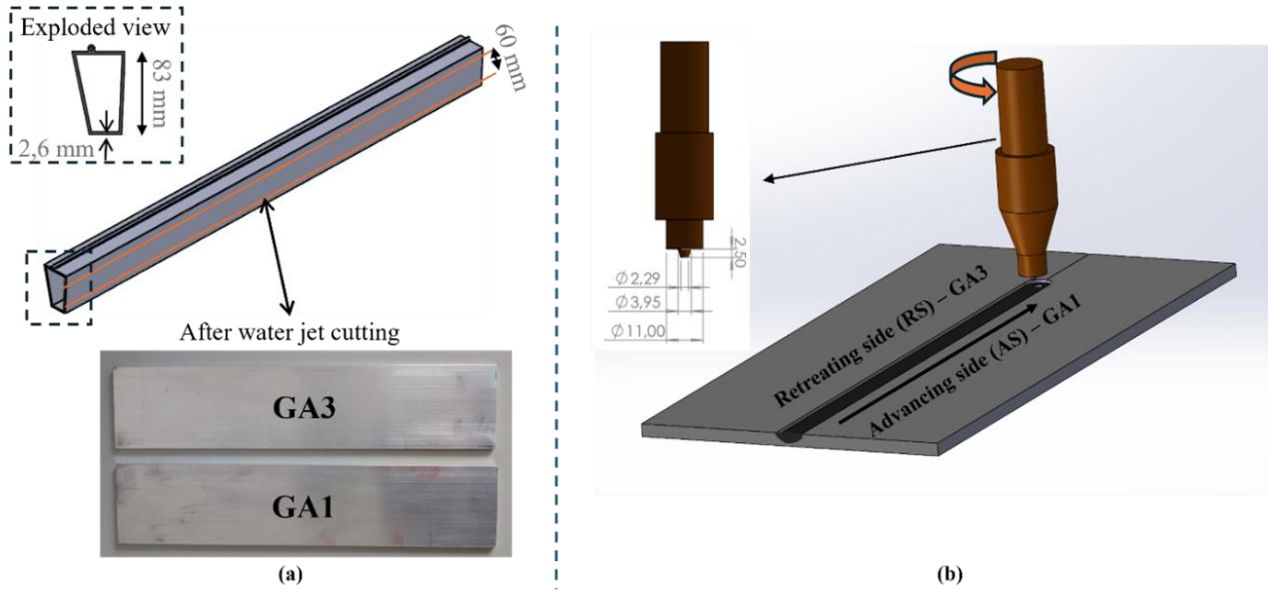

Figure 1 Outline of the experimental setup used in the FSW trials**:** (a) Sheet preparation, (b) Tool design and welding conditions

2.2 Characterization of base metals and welds

Prior to the weld characterization, anisotropy in the BMs' mechanical properties was evaluated individually. The sample extraction plan for the tensile studies is illustrated in **Figure 2(a)** & **2(b)**, respectively. Rectangular tensile specimens (gauge length: 15 mm, total length: 40 mm) were extracted from each BM with orientations 0°, 45°, and 90° relative to the extrusion direction using an electrical discharge machine (EDM). Tensile testing was conducted using a Step Lab – Multiaxial 20 kN machine at a quasi-static strain rate of 10^{-3} s^{-1}. The true strains in different directions ε_x, ε_y, and ε_z were measured from the tested tensile specimens, while the plastic strain ratio, r_α, is calculated using Equation 1 [12]. Subsequently, the normal, $\bar{R}$, and planar, ΔR, anisotropies were calculated using Equations 2 & 3 for GA1 and GA3 individually [12].

$$r_\alpha = \left(\frac{\varepsilon_y}{\varepsilon_z}\right)_\alpha \tag{1}$$

$$\bar{R} = \frac{r_0 + 2r_{45} + r_{90}}{4} \tag{2}$$

$$\Delta R = \frac{r_0 - 2r_{45} + r_{90}}{2} \tag{3}$$

Similarly, the tensile properties of the SZ were evaluated by extracting sub-sized tensile samples within the welded region of the TWB (WL || ED). In this case, it is reasonable to assume that as long as the welding parameters are kept constant, the properties of the SZ will not differ significantly with respect to weld line orientation. Moreover, the transverse tensile properties of the TWBs were evaluated by extracting tensile specimens (gauge length: 25 mm, total length: 100 mm) perpendicular to the weld line for all three orientations. A range of 3-5 samples was used in these tensile studies to increase statistical significance in the measurements. Microhardness was measured in the cross section of TWBs using a Mitutoyo HM-200 Vickers hardness tester at 0.5 mm depth from the top surface, applying a load of 0.1 kg and a dwell time of 10 seconds.

Prior to the metallographic examination, the BMs and SZ were sectioned and polished using emery papers (500–4000 grits), diamond pastes (9, 3, 1 µm), and colloidal silica. Subsequently, electropolishing was done in a 10% perchloric acid–90% methanol solution at 20 V for 15 seconds. The electron backscattered diffraction (EBSD) analysis was performed on the electro-polished samples, and inverse pole figure (IPF) maps were constructed using FEI-Quanta 650 FEG Scanning Electron Microscope (SEM) to reveal the grain orientations and phase distribution within the recrystallized surface layers of the BMs and the SZ of the welds.

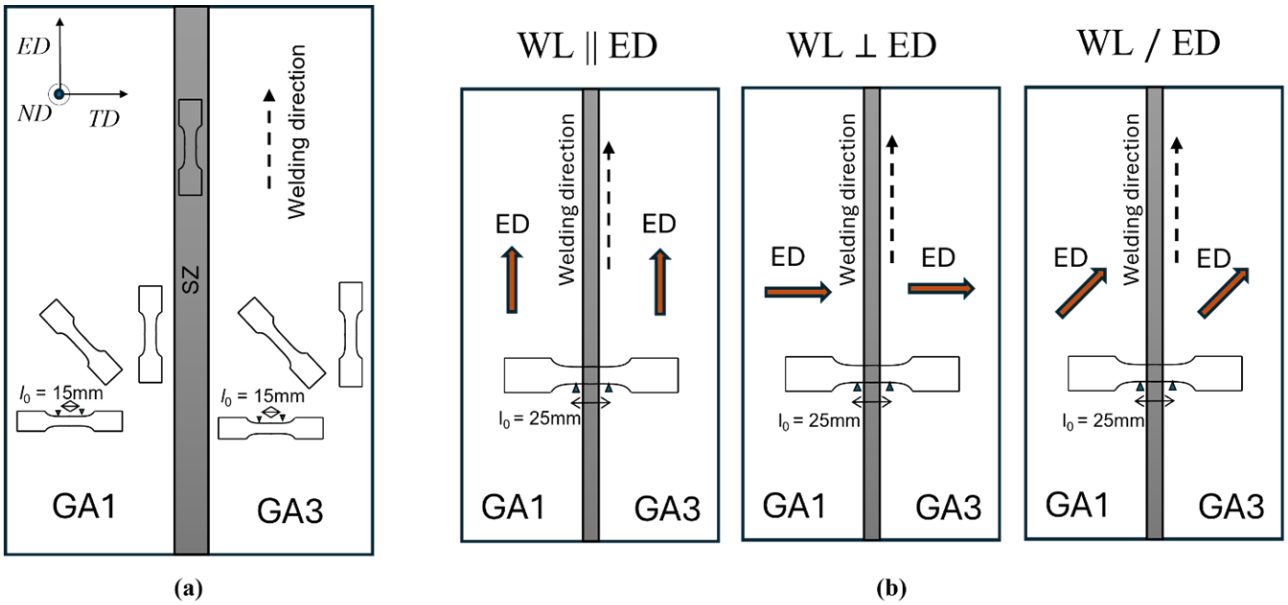

Figure 2 Sample extraction plan for the tensile studies: (a) Orientations of the tensile specimens extracted from BMs and SZ, (b) Location of the transverse tensile specimens extracted from TWBs with respect to the different weld line orientations

3. RESULTS AND DISCUSSION

3.1 Comparison of mechanical properties and microstructure between the BMs and the SZ

The BMs' engineering stress-strain curves are displayed in **Figure 3(a)** & **3(b)**, respectively. The resulting ultimate tensile strength (UTS), yield strength (YS), and elongation (% El.), along with the data for the anisotropy of the BMs, are tabulated below the graphs. UTS and YS are generally higher in the extrusion direction, while the elongation is higher in the transverse direction for both BMs. GA3 showed increased strength and reduced ductility due to its higher Cu and Fe contents. This is because Cu promotes the formation of hardening precipitates during age hardening, whereas Fe leads to the formation of Fe-rich intermetallics [13]. Significant differences in mechanical anisotropy are observed between the BMs. GA3 showed higher values of planar anisotropy (ΔR = 1.066) and normal anisotropy ($\bar{R}$ = 1.86) compared to GA1 (ΔR = 0.342 and $\bar{R}$ = 1.09). These differences are probably due to variations in the texture between the BMs in the through-thickness direction [14]. Crystallographic texture is primarily influenced by the composition, distribution, and number density of different phases within the material. In the previous study of the same BMs [15], significant differences in the distribution and number density of Fe-rich intermetallic particles were reported between GA1 and GA3. The number density of Al-Fe-Mn-Si intermetallic particles was generally higher at the surface compared to the centre of the extrusions. Specifically, it was highest in GA3, being rich in Fe and Cu.

The engineering stress-strain curve for the SZ, taken from the TWB (WL || ED), is provided in **Figure 3(c).** SZ demonstrated equivalent UTS compared to both the BMs, which is usually not observed in friction stir welded

Al alloys. Furthermore, there is a significant drop in YS, which is accompanied by an increase in elongation. The YS decreased by approximately 40% compared to the BM value, reducing to 195 MPa. In general, solute elements, hardening precipitates, and dispersoids contribute to the YS in aluminum alloys [16, 17]. However, the imposed thermal cycle during the welding operation leads to full dissolution of hardening precipitates and promotes DRX behavior. This increases the solute content in the Al matrix, thus contributing to a low YS after subsequent natural aging. However, it enhances work-hardening and UTS during tensile testing due to a reduced dynamic recovery rate. At the same time, the elongation of the SZ increased to approximately 1.7 times that of the BM value. The volume fraction and distribution of intermetallic constituent particles also influence the ductility of the SZ [18]. These particles do not melt during FSW, as their melting temperatures significantly exceed the peak temperatures reached during the welding process. However, they undergo fragmentation and get redistributed within the Al matrix. This refinement of their spatial distribution leads to a further increase in the fracture strain of the SZ compared to the BMs.

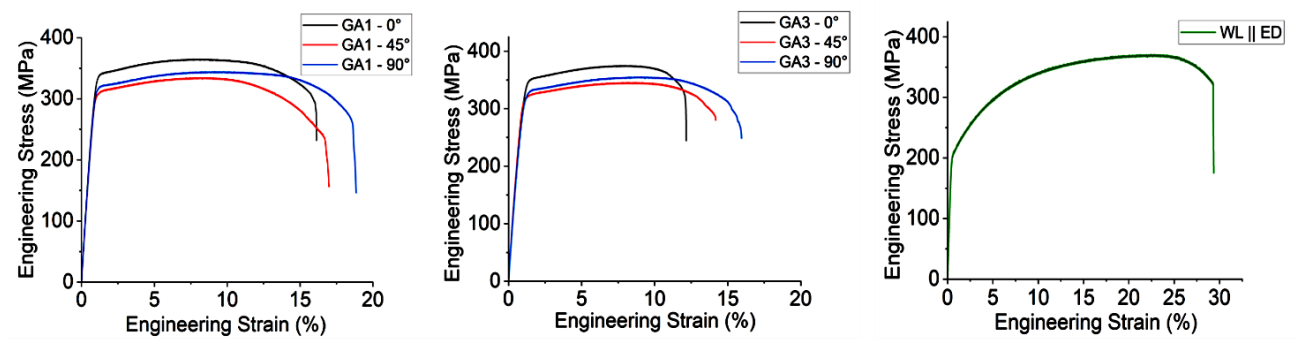

GA1 - Primary AA6082				
Direction	UTS (MPa)	YS (MPa)	% El.	Anisotropy
0°	365 ± 5	332 ± 4	16 ± 0,9	
45°	334 ± 9	315 ± 3	17 ± 0,5	$\bar{R}$ = 1.09 ΔR = 0.342
90°	344 ± 4	321 ± 6	19 ± 0,5	

(a)

GA3 - Recycled AA6082				
Direction	UTS (MPa)	YS (MPa)	% El.	Anisotropy
0°	375 ± 6	343 ± 5	12 ± 0,2	
45°	355 ± 11	315 ± 6	16 ± 0,4	$\bar{R}$ = 1.86 ΔR = 1.066
90°	345 ± 7	299 ± 8	15 ± 0,8	

(b)

SZ			
Direction	UTS (MPa)	YS (MPa)	% El.
WL || ED	370 ± 10	195 ± 8	29 ± 1

(c)

Figure 3 Compilation of different engineering stress-strain curves; (a) GA1 - Primary AA6082, (b) GA3 - Recycled AA6082 & (c) SZ – extracted from the WL || ED weld

The microstructural differences between the BMs and the SZ were examined using SEM-EBSD, and the corresponding IPF maps are presented in **Figure 4(a-c)**, respectively. The average grain size in the recrystallized surface layers of GA1 and GA3 varies between 20 – 25 µm. The corresponding recrystallized grains in the SZ are much finer, and their average size varies between 4 – 10 µm for all orientations. In terms of morphology, the SZ grains are equiaxed compared to the flat, elongated grains in the BMs oriented in the extrusion direction. Note that the grain size variation in the SZ for the different weld line orientations was found to be statistically insignificant, as their grain size distributions tend to overlap. This was confirmed after EBSD studies in all three orientations within the SZ. However, a variation in the grain size in the through-thickness direction was observed, varying from 10 µm at the top to 4 µm at the bottom. During welding, higher temperatures and intense stirring near the tool shoulder lead to grain coarsening, while the cooler and more uniformly strained region around the submerged tool pin promotes finer grains. This result is also consistent with that reported by other researchers [3, 5].

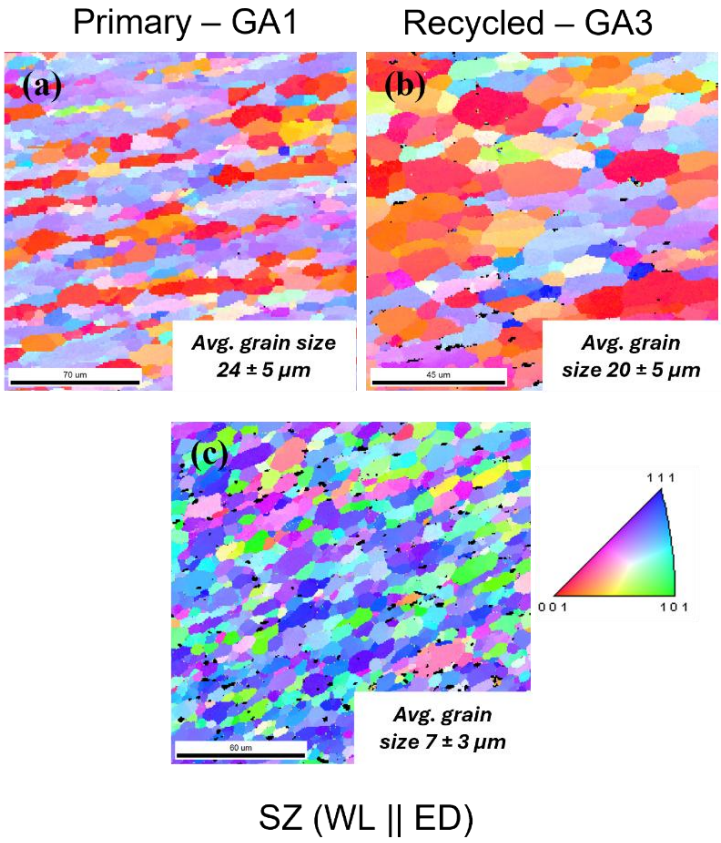

Figure 4 Variation in recrystallized grain size between the BMs (a & b) and the SZ (c) in the WL || ED weld

3.2 Microhardness and transverse properties of TWBs in different weld line orientations

The results of the microhardness measurements of TWBs welded in different orientations are shown in **Figure 5**. The hardness profiles exhibit a characteristic W-shaped pattern, with the soft HAZ located on both sides of the weld, as commonly observed after FSW of age-hardened Al-Mg-Si alloys. Typically, the HAZ located on the AS displays a much lower hardness than the RS, with measured values varying with the weld line orientation. The lower hardness was observed in the WL/ED weld, which revealed a value of 55 HV on the AS. For the other weld orientations, this ranged between 60 – 70 HV. While the HAZ showed the most significant softening, notable differences in hardness were also evident across the BMs and the SZ. The hardness values of the BMs varied between 100 – 120 HV. Compared to the BMs, the hardness values in the SZ were relatively lower. Especially, the peak hardness within the SZ appeared to be orientation-dependent, with values ranging from 70 to 90 HV. Overall, the higher hardness was observed for the WL || ED weld, whereas the lower hardness was observed for the WL / ED weld. This is because the heat generated and the extent of DRX will vary, depending on the orientation of the base metals with respect to the weld line during FSW [19]. As a consequence, the corresponding hardness values in the HAZ will also vary with weld line orientation.

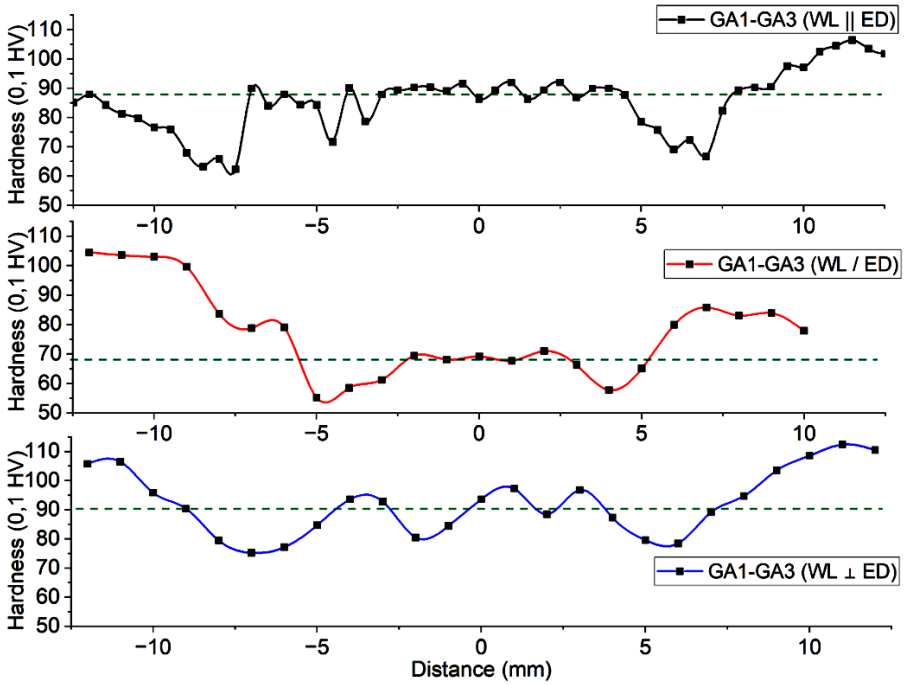

Figure 5 Hardness profile for TWBs in different weld line orientations

The differences in the transverse tensile properties of the TWBs for all three weld line orientations are illustrated by the engineering stress-strain curves and tabulated values in **Figure 6**. The results reveal that the transverse mechanical response is largely unaffected by the weld line orientation, with both the strength and the ductility nearly identical for all weld configurations. Especially, the UTS and elongation at fracture were relatively lower than those of the BMs, with UTS values around 200 MPa, and elongation approximately 8.0%. Note that the failure occurred in the HAZ located on the AS in all three orientations in the tensile tests. This failure location is consistent with the results from the transverse hardness measurements shown in **Figure 5**. The minimum HAZ hardness was always observed in the AS of the welds, triggering strain localization and necking in that region during tensile deformation, resulting in premature failure.

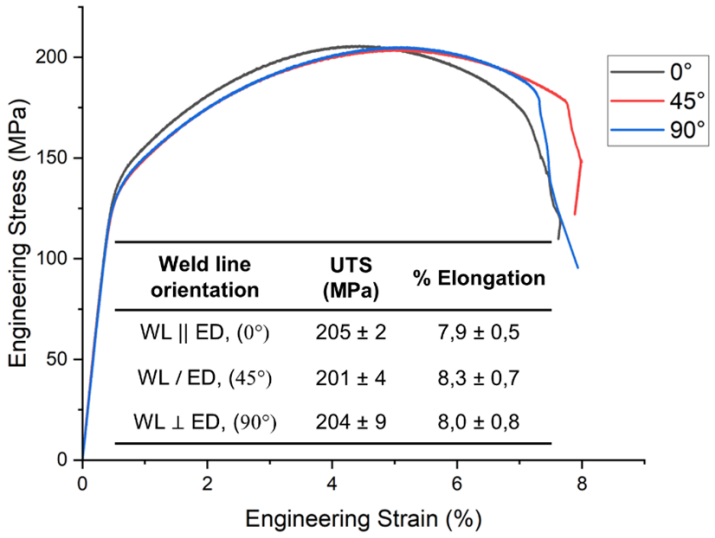

Figure 6 Transverse tensile properties of TWBs for different weld line orientations

4. CONCLUSION

This study investigates the friction stir welding (FSW) of both primary and recycled 6082 aluminum alloys, focusing on how the orientation of the weld line influences the resulting mechanical properties. The main results from this study can be summarized as follows:

- The compositions of the BMs, particularly their different Fe and Cu contents, influence their mechanical properties, especially mechanical anisotropy, which was mainly governed by the distribution and number density of intermetallic phases through the material thickness.
- The stir zone of the welds exhibited lower yield strength and higher ductility than the BMs. This is due to the dissolution of strengthening precipitates and the homogenization of intermetallic phases after welding. The increase in the solute content enhances work hardening, which causes an increase in UTS during tensile testing.
- The peak hardness within the SZ is sensitive to weld line orientation, showing a maximum hardness ranging between 70 and 90 HV.
- Weld line orientation had minimal influence on the transverse tensile strength and elongation, which remained consistently lower than the BMs. Failure occurred in the HAZ located on the AS in all three orientations.

ACKNOWLEDGEMENTS

The authors gratefully acknowledge the financial support from the Norwegian University of Science and Technology (NTNU), NTNU Aluminum Product Innovation Center (NAPIC), and the Alu Green project (No: 328831) sponsored by the Research Council of Norway.

REFERENCES

[1] DEBROY, T., BHADESHIA, H. Stirring solid metals to form sound welds. *Innovations in Everyday Engineering Materials*. 2021, pp. 21-34.

[2] SHAH, P.H., BADHEKA, V.J. Friction stir welding of aluminum alloys: an overview of experimental findings–process, variables, development and applications. *Proceedings of the Institution of Mechanical Engineers, Part L: Journal of Materials: Design and Applications*. 2019, vol. 233, pp. 1191-1226.

[3] MISHRA, R.S., MA, D.Z. Friction stir welding and processing. *Materials science and engineering: Reports*. 2005, vol. 50, pp. 1-78.

[4] NANDAN, R., DEBROY, T., BHADESHIA, H. Recent advances in friction-stir welding–process, weldment structure and properties. *Progress in Materials Science*. 2008, vol. 53, pp. 980-1023.

[5] THREADGILL, P., LEONARD, A., SHERCLIFF, H., WITHERS, P. Friction stir welding of aluminum alloys. *International Materials Reviews*. 2009, vol. 54, pp. 49-93.

[6] YAKUBOV, V., OSTERGAARD, H., BHAGAVATH, S., LEUNG, C.L.A., HUGHES, J., YASA, E., KHEZRI, M., LOSCHKE, S.K., LI, Q., PARADOWSKA, A.M. Recycled aluminum feedstock in metal additive manufacturing: A state of the art review. Heliyon 2024, 10, e27243. https://doi.org/10.1016/j.heliyon.2024.e27243.

[7] LIU, X., CAI, Z., MING, M., HOU, Q., LUAN, X., LIU, H., ZHANG, L., POLITIS, D.J., DU, Q., WANG, L. Fast light alloy stamping technology (FAST) for manufacturing lightweight pressings from dissimilar aluminum alloy-tailor welded blanks. Journal of Manufacturing Processes 2024;120:1141-1156.

[8] KRISHNAMRAJU, M., REDDY, P.V., APPALANAIDU, B., MARKENDEYA, R. Mechanical behavior and forming characteristics of tailor-welded blanks of structural materials: a review. *Multiscale and Multidisciplinary Modeling, Experiments and Design*. 2024, vol. 7, pp. 3133-3151.

[9] SIDDARTHAN, M. Y.R., LIU, X., MA, J., WELO, T., GRONG, Ø. Friction-stir, tailor-welded blanks made from primary and recycled 6082 aluminum alloys. *Manufacturing Letters*. 2025

[10] BUSTE, A., LALBIN, X., WORSWICK, M.J., CLARKE, J.A., ALTSHULLER, B., FINN, M., JAIN, M. Prediction of strain distribution in aluminum tailor welded blanks for different welding techniques. *Canadian Metallurgical Quarterly*. 2000, vol. 39, pp. 493-501. https://doi.org/10.1179/cmq.2000.39.4.493.

[11] SIDDARTHAN, M Y.R., MA, J., LIU, X.C., WELO, T., GRONG, Ø. Friction-stir, tailor-welded blanks made from primary and recycled 6082 aluminum alloys (submitted for publication). *Manufacturing Letters*. 2025

[12] NARAYANASAMY, R., NARAYANAN, C.S. Forming limit diagram for interstitial free steels - Part I. *Materials Science and Engineering a-Structural Materials Properties Microstructure and Processing*. 2005, vol. 399, pp. 292-307. https://doi.org/10.1016/j.msea.2005.04.004.

[13] LU, Q., LU, K., CHEN, H.N., YANG, M.J., LAN, X.Y., YANG, T., LIU, S.H., SONG, M., CAO, L.F., DU, Y. Simultaneously enhanced strength and ductility of 6xxx Al alloys via manipulating meso-scale and nano-scale structures guided with phase equilibrium. *Journal of Materials Science & Technology*. 2020, vol. 4, pp. 139-148. https://doi.org/10.1016/j.jmst.2019.09.029.

[14] BARNWAL, V.K., RAGHAVAN, R., TEWARI, A., NARASIMHAN, K., MISHRA, S.K. Effect of microstructure and texture on forming behaviour of AA-6061 aluminum alloy sheet. *Materials Science and Engineering a-Structural Materials Properties Microstructure and Processing*. 2017, vol. 679, pp. 56-65. https://doi.org/10.1016/j.msea.2016.10.027.

[15] SARKAR, A., AKTUNALI, M., ARBO, S.M., HOLMESTAD, J., VIESPOLI, L.M., NYHUS, B.G.R., RAZAVI, N. A study on the influence of impurity content on fatigue endurance in a 6082 Al-alloy. *International Journal of Fatigue*. 2024, vol. 186, p. 108406. https://doi.org/10.1016/j.ijfatigue.2024.108406 .

[16] MYHR, O.R., GRONG, Ø, PEDERSEN, K.O. A combined precipitation, yield strength, and work hardening model for Al-Mg-Si alloys. *Metallurgical and Materials Transactions A*. 2010, vol. ;41, pp. 2276-2289.

[17] PEDERSEN, K.O., WESTERMANN, I., FURU, T., BØRVIK, T., HOPPERSTAD, O.S. Influence of microstructure on work-hardening and ductile fracture of aluminum alloys. *Materials & Design*. 2015, vol. 70, pp. 31-44.

[18] HANNARD, F., CASTIN, S., MAIRE, E., MOKSO, R., PARDOEN, T., SIMAR, A. Ductilization of aluminum alloy 6056 by friction stir processing. *Acta Materialia*. 2017, vol. 130, pp. 121-136.

[19] BARBINI, A., CARSTENSEN, J., DOS SANTOS, J.F. Influence of alloys position, rolling and welding directions on properties of AA2024/AA7050 dissimilar butt weld obtained by friction stir welding. *Metals*. 2018, vol. 8, p. 202. https://doi.org/10.3390/met8040202.